PHYSICAL REVIEW B **94**, 081302(R) (2016)

Anisotropic and strong negative magnetoresistance in the three-dimensional topological insulator Bi_2Se_3

S. Wiedmann,[1,*] A. Jost,[1] B. Fauqué,[2] J. van Dijk,[1] M. J. Meijer,[1] T. Khouri,[1] S. Pezzini,[1] S. Grauer,[3] S. Schreyeck,[3] C. Brüne,[3] H. Buhmann,[3] L. W. Molenkamp,[3] and N. E. Hussey[1]

[1]*High Field Magnet Laboratory (HFML-EMFL) & Institute for Molecules and Materials, Radboud University, Toernooiveld 7, 6525 ED Nijmegen, The Netherlands*

[2]*LPEM (CNRS-UPMC), ESPCI, 75005 Paris, France*

[3]*Physikalisches Institut (EP3), Universität Würzburg, Am Hubland, 97074 Würzburg,Germany*

(Received 15 April 2016; revised manuscript received 18 July 2016; published 10 August 2016)

We report on high-field angle-dependent magnetotransport measurements on epitaxial thin films of Bi_2Se_3, a three-dimensional topological insulator. At low temperature, we observe quantum oscillations that demonstrate the simultaneous presence of bulk and surface carriers. The magnetoresistance of Bi_2Se_3 is found to be highly anisotropic. In the presence of a parallel electric and magnetic field, we observe a strong negative longitudinal magnetoresistance that has been considered as a smoking gun for the presence of chiral fermions in a certain class of semimetals due to the so-called axial anomaly. Its observation in a three-dimensional topological insulator implies that the axial anomaly may be in fact a far more generic phenomenon than originally thought.

DOI: 10.1103/PhysRevB.94.081302

The role of topology in condensed matter systems, once a rather esoteric pursuit, has undergone a revolution in the last decade with the realization that a certain class of insulators and semimetals play host to topologically protected surface states. In 2009, band structure calculations revealed that stoichiometric Bi_2Se_3, a well-known thermoelectric material [1], bears all the hallmarks of a three-dimensional topological insulator (3D TI) [2] with an insulating bulk and conducting surface states provided that the Fermi energy ϵ_F is situated within the bulk band gap [3]. These gapless surface states possess opposite spin and momentum, and are protected from backscattering by time reversal symmetry. The existence of Dirac-like surface states within the bulk band gap was confirmed in an angle-resolved photoemission spectroscopy study performed that same year [4].

Though Bi_2Se_3 is arguably the most simple representative of the 3D TI family, accessing the topological surface states (TSS) in transport has been hindered by a large residual carrier density in the bulk [5,6]. While Shubnikov–de Haas (SdH) oscillations are a powerful means to distinguish between bulk and surface charge carriers via their angle dependence, their analysis and interpretation remain controversial. The literature is replete with results that have been attributed to single bands of bulk carriers, TSS, or multiple bands, emphasizing the difficulty in distinguishing between the bulk, TSS, and a two-dimensional charge-accumulation layer [5–11]. Apart from the TSS, the electronic bulk states in Bi_2Se_3 are of particular interest since their spin splitting is found to be twice the cyclotron energy observed in quantum oscillation [12,13] and optical [14] experiments. Another peculiar property of Bi_2Se_3 and other 3D TIs is the observation of a linear positive magnetoresistance (MR) that persists up to room temperature [15–20].

The recent explosion of interest in 3D massless Dirac fermions in "3D Dirac" or "Weyl" semimetals [21] is based primarily on their unique topological properties that can be revealed in relatively straightforward magnetotransport experiments. Examples include the observation of an extremely large positive MR [22], linear MR [23], and, more specifically, the negative longitudinal MR (NLMR) predicted to appear in Weyl semimetals when the magnetic and electric field are coaligned. This NLMR has been attributed to the axial anomaly, a quantum mechanical phenomenon that relies on a number imbalance of chiral fermions in the presence of an applied electric field [22,24–26]. In a recent theoretical study, however, it was proposed that the NLMR phenomenon may in fact be a generic property of metals and semiconductors [27], rather than something unique to topological semimetals.

In this Rapid Communication, we present magnetotransport experiments on Bi_2Se_3 epitaxial layers in magnetic fields up to 30 T. At low temperatures, we establish the existence of both bulk and surface carriers via angle-dependent SdH measurements. Moreover, we observe a strong anisotropy in the MR which depends on the orientation of the current I with respect to the applied magnetic field B over a wide range of carrier concentrations. When the magnetic field is applied parallel to I ($I \parallel B_x$), we observe a strong NLMR. This surprising finding confirms that the observation of NLMR is not unique to Weyl semimetals and therefore cannot by itself be taken as conclusive evidence for the existence of Weyl fermions in other systems. With this in mind, we consider possible alternative origins of this increasingly ubiquitous phenomenon, but argue finally that the axial anomaly may indeed be generic to a host of three-dimensional materials [27].

The present study has been performed on samples with different layer thicknesses $d = 290$, 190, 50, and 20 nm (referred to hereafter as samples A, B, C, and D) grown by molecular beam epitaxy (MBE) on an InP(111)B substrate [28] and patterned in a six-terminal Hall-bar geometry [length $L \times$ width W, (30×10) μm^2]. The carrier concentration $n = n_{\mathrm{Hall}}$ at 300 K (extracted from the linear part of the low-field Hall resistivity ρ_{xy}) varies from 1.2×10^{18} to 1.7×10^{19} cm^{-3} with decreasing thickness [29]. All magnetotransport measurements reported here were performed in a ^{4}He flow cryostat in

*s.wiedmann@science.ru.nl

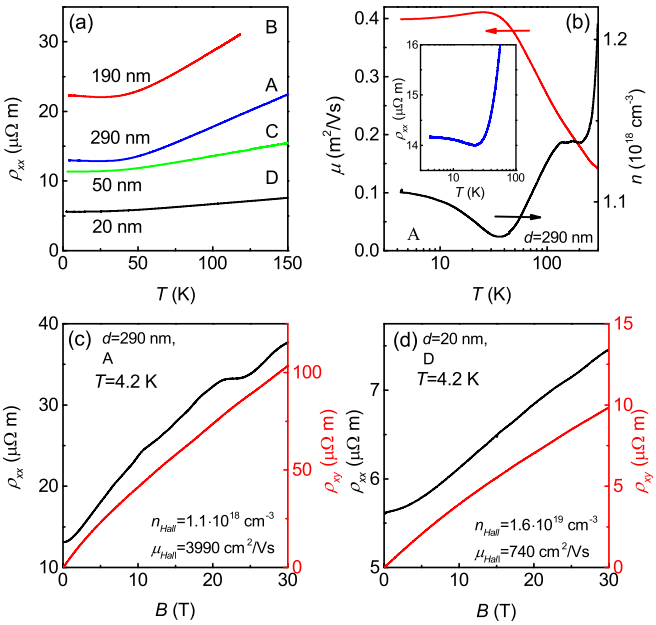

FIG. 1. (a) Temperature dependence of the electrical resistivity ρ_{xx} for Bi_2Se_3 MBE-grown films with different thicknesses. (b) Mobility μ and carrier density n as a function of T for sample A. (c), (d) ρ_{xx} and ρ_{xy} as a function of B at $T = 4.2$ K for A and D, respectively. The quoted carrier density is extracted from the low-field Hall resistance.

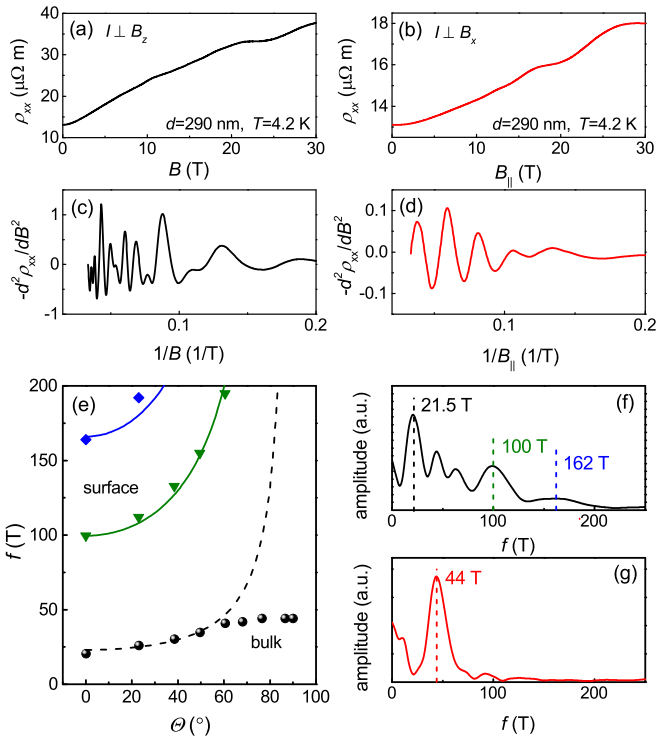

FIG. 2. Longitudinal resistivity ρ_{xx} as a function of (a) perpendicular and (b) in-plane magnetic field at 4.2 K for sample A, respectively. (c), (d) Second derivative of $\rho_{xx}(B)$ as a function of $1/B$ and $1/B_{\|}$ to highlight the SdH oscillations. (e) Extracted frequencies from the FFT analysis as a function of angle showing contributions from surface and bulk carriers. The straight (dashed) lines correspond to the $1/\cos\Theta$ dependence expected for a purely two-dimensional system. (f), (g) FFTs for a perpendicular and parallel field sweep, respectively, with the primary oscillation frequencies highlighted.

a resistive (Bitter) magnet up to 30 T using standard ac lock-in detection techniques with an excitation current of 1 μA. For the SdH oscillation analysis, the magnetic field is applied in a plane perpendicular to the current I.

The temperature dependence of the longitudinal resistivity ρ_{xx} is shown in Fig. 1(a) for all four samples. In Fig. 1(b), we plot the carrier mobility μ and concentration $n = 1/(R_H e)$ for sample A obtained from the zero-field $\rho_{xx}(T)$ sweep and the measured ρ_{xy} at $B = 1$ T, respectively. The overall temperature dependence is metallic ($dR_{xx}/dT > 0$), though below 40 K we observe a tiny upturn in ρ_{xx} which is strongest for the sample with the lowest carrier density. This increase is accompanied by a small decrease in μ and an apparent increase in n which has been interpreted to originate from the presence of an impurity band [7,8,30]. In Figs. 1(c) and 1(d), we plot ρ_{xx} and ρ_{xy} as a function of the magnetic field B up to 30 T for samples A and D. SdH oscillations are superimposed on top of a positive quasilinear MR while ρ_{xy} is found to be nonlinear for $B > 2$ T, suggesting the possible presence of two carrier types. From the low-field ρ_{xy}, we extract a carrier mobility of 3990 (740) $\mathrm{cm}^2/\mathrm{V\,s}$ for sample A (D), respectively.

We now turn to focus on the observation of quantum oscillations which is presented in Fig. 2 for the sample with the highest carrier mobility (A). In Figs. 2(a) and 2(b), we show $\rho_{xx}(B)$ at 4.2 K when subject to an out-of-plane and in-plane magnetic field. Quantum oscillations are clearly visible in the second derivative $-d^2\rho_{xx}/dB^2$, respectively, as a function of the inverse field, plotted in Figs. 2(c) and 2(d) for both orientations. In the parallel field configuration, only one frequency is evident, whereas several frequencies are found in a perpendicular field.

In order to identify the origin of the quantum oscillations, we have performed fast Fourier transforms (FFTs) on a series of ρ_{xx} curves measured at different tilt angles Θ. The results are summarized in Fig. 2(e). For $\Theta = 0$ (perpendicular field configuration), we observe three frequencies at 21.5, 100, and 162 T [see Fig. 2(f)]. All frequencies appear to follow a $1/\cos\Theta$ up to tilt angles of around 60°, characteristic of a two-dimensional electronic state. Beyond 60°, however, the lower frequency starts to deviate from this behavior and saturates towards 90°. We therefore attribute the observed frequencies to two surface states (top and bottom) and one bulk band. Taking the Onsager relation, i.e., the extremal cross section of the Fermi surface $A(E_F) \propto f$, and assuming an ellipsoid pocket with $V = 4/3\pi a^2 b$, we obtain $n_{\mathrm{bulk}} = 8.1 \times 10^{17}\,\mathrm{cm}^{-3}$ for the bulk band corresponding to the pocket with the lowest frequency. For the surface states, we obtain the carrier densities 2.4×10^{12} and $3.9 \times 10^{12}\,\mathrm{cm}^{-2}$. From the quantum oscillation analysis, we thus obtain a total carrier concentration of $n_{\mathrm{tot,SdH}} = 1.0 \times 10^{18}\,\mathrm{cm}^{-3}$, in excellent agreement with n_{Hall}. In contrast, assuming that all three pockets were ellipsoidal (i.e., bulk), we would obtain a total carrier concentration that is one order of magnitude larger than n_{Hall}.

Let us now turn our attention to the peculiar MR we observe in these samples. To avoid quantum oscillatory and quantum interference phenomena [29], we first focus here on

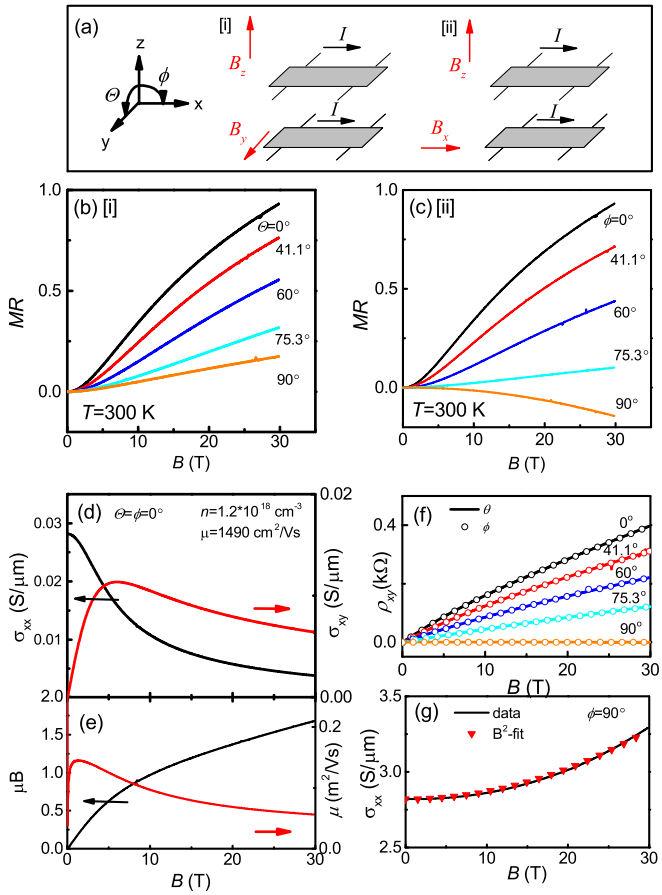

FIG. 3. Anisotropic magnetotransport in Bi_2Se_3 at $T = 300$ K: (a) Schematic diagram of the electrical transport measurements for configurations [i] and [ii]. (b), (c) Magnetoresistance of sample A as a function of B for both configurations, indicating a strong negative MR if $I \parallel B_x$. (d) Longitudinal σ_{xx} and Hall conductivities σ_{xy} as a function of the magnetic field and (e) extracted μB and μ using the Drude model. (f) Hall resistivity ρ_{xy} as a function of B for both configurations (solid line for [i], open symbols for [ii]). (g) The conductivity σ_{xx} as a function of B (solid line) at $\phi = 90^\circ$ is found to be $\propto B^2$ (triangles).

the angle-dependent MR response at room temperature. The longitudinal and Hall resistivities have been measured in two different configurations, as shown in Fig. 3(a). In configuration [i], the applied magnetic field is always perpendicular to I (field rotated in the orthogonal plane) whereas in configuration [ii], the current and field are parallel if $\phi = 90^\circ$. The carrier concentrations (mobilities) extracted from ρ_{xy} (ρ_{xx}) at low fields are summarized in Table I in the Supplemental Material [29].

We first present our results and analysis for the high mobility sample (A) in Fig. 3. In Figs. 3(b) and 3(c), we plot the MR $= [\rho_{xx}(B) - \rho_0]/\rho_0$ at different angles Θ and ϕ, as indicated in each figure. The overall MR is similar to the one observed at low temperature, i.e., it first increases quadratically then tends towards saturation at a higher field. In both configurations, the MR is strongly anisotropic. Most surprisingly, we observe a large NLMR (∼15%) when the magnetic field is applied parallel to the current ($I \parallel B_x$). As the second bulk conduction band is far from the Fermi energy ϵ_F at room temperature [30–32], we analyze the MR at $\Theta = \phi = 0$ using a standard one-carrier Drude model (for completeness, a two-carrier analysis is presented in the Supplemental Material [29]).

The corresponding longitudinal and Hall conductivities σ_{xx} and σ_{xy} in the transverse configuration are illustrated in Fig. 3(d). From ρ_{xy}/ρ_{xx} we extract μB and finally the carrier mobility μ as a function of the applied field, as shown in Fig. 3(e), and find that $\mu(0\ \mathrm{T})/\mu(30\ \mathrm{T}) \simeq 2.7$. Based on this simple analysis, we can infer that the mobility and corresponding scattering time strongly depend on the magnetic field. We have also measured the dependence of ρ_{xy} for both configurations and found that the Hall resistivity follows a simple cosine dependence and does not depend on the orientation of B with respect to I [see Fig. 3(f)]. Finally, in Fig. 3(g), we plot $\sigma_{xx}(B)$ for the parallel field configuration ($I \parallel B_x$, solid line) and observe a B^2 dependence up to 30 T [symbols represent a quadratic fit $\sigma_{xx}(B) = \sigma_0 + aB^2$ to the data].

In Fig. 4(a), we present the temperature dependence of the normalized longitudinal magnetoresistivity $\rho_{xx}(B)/\rho_{xx}(0)$ for

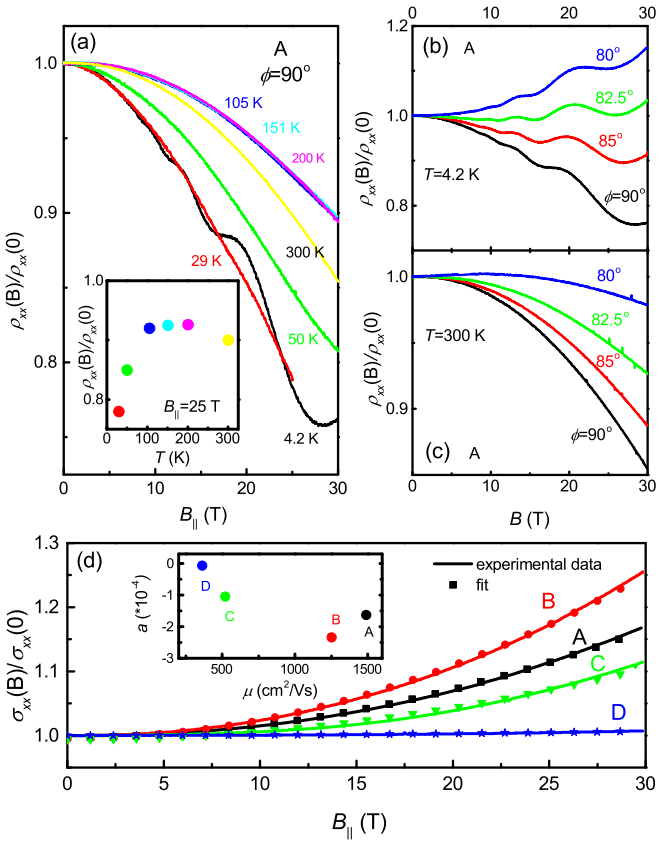

FIG. 4. (a) Normalized longitudinal magnetoresistivity $\rho_{xx}(B)/\rho_{xx}(0)$ for sample A at different temperatures [inset: $\rho_{xx}(B)/\rho_{xx}(0)$ at $B = 25$ T]. $\rho_{xx}(B)/\rho_{xx}(0)$ for different angles ϕ at (b) $T = 4.2$ K and (c) $T = 300$ K. (d) Normalized magnetoconductivity $\sigma_{xx}(B)/\sigma_{xx}(0)$ at $T = 300$ K for all samples A, B, C, and D for $\phi = 90^\circ$. All samples follow a $\sigma_{xx}(B)/\sigma_{xx}(0) \propto B^2$ dependence (see fits). The inset shows the fitting parameter a as a function of μ for all samples.

several chosen temperatures for sample A. With increasing temperature, the NLMR becomes slightly weaker, is constant in the range between 100 and 200 K, and increases again at 300 K, as shown in the inset to Fig. 4(a). In Figs. 4(b) and 4(c), we plot $\rho_{xx}(B)/\rho_{xx}(0)$ for sample A at 4.2 and 300 K, respectively, when an additional perpendicular magnetic field is applied. The NLMR turns into a positive one by adding a small out-of-plane component at $\phi \simeq 83^\circ$ ($\phi < 80^\circ$) for 4.2 K (300 K). At 4.2 K, the NLMR is superimposed by SdH oscillations which have previously been attributed to TSS from the sidewalls [33]. We have shown here, however, that they originate from the lowest bulk conduction band.

The anisotropy in the MR and the large NLMR in a parallel field are not unique to one particular wafer or sample. Indeed, for all samples, we observe a positive MR in a purely perpendicular magnetic field and a NLMR in the longitudinal configuration [29]. Moreover, for the samples (C and D) with the lowest carrier mobility, a negative MR is also observed for $I \perp B_y$. The negative MR for $I \perp B_y$ can be explained using the classical Drude model provided the bulk carriers have a low mobility [29]. In Fig. 4(a), we plot $\sigma_{xx}(B)/\sigma_{xx}(0)$ as a function of $B_\parallel$ and find that the NLMR gets progressively weaker with decreasing d (increasing carrier concentration and decreasing carrier mobility) at room temperature. Significantly, the longitudinal conductivity follows the B^2 behavior for all samples [the fitting parameter a as a function of μ is shown in the inset of Fig. 4(d) for all samples].

Standard Boltzmann theory does not predict any longitudinal magnetoresistance in the presence of a magnetic field that is parallel to the applied electric field. A NLMR has been observed previously in both one-dimensional (1D) [34] and two-dimensional (2D) [35] charge ordered systems for currents applied parallel to the conducting chains (planes). In both cases, the NLMR exhibited $(B/T)^2$ scaling attributed to a closing of the charge gap due to Zeeman splitting. In Bi_2Se_3, by contrast, there is no strong T dependence in the NLMR. A classical origin, found in inhomogeneous conductors and attributed to macroscopic inhomogeneities and thus distorted current paths [36], can be excluded since the anisotropic MR does not depend on the lateral sample size [37]. The origin of the anisotropy of the MR and, in particular, the large NLMR in Bi_2Se_3 is likely to arise from the underlying scattering mechanism, as inferred from our simple Drude analysis. In 1956, Argyres and Adam predicted a NLMR for a 3D electron gas in the case of nondegenerate semiconductors where ionized impurity scattering is present [38], as observed, for example, in indium antimonide in the extreme quantum limit [39]. In contrast, recently triggered by the discovery of new Dirac materials [22–26], it has been proposed that a quantum mechanical phenomenon called the axial anomaly can give rise to a NLMR [27]. In a magnetic field, charge carriers are subject to Landau quantization with a 1D dispersion along B. If, in addition, an electric field is applied parallel to B, a uniform acceleration of the center of mass in this field-induced 1D system produces the same axial anomaly effect as charge pumping between Weyl points in a Weyl semimetal and the subsequent charge imbalance leads to a NLMR [22,27]. This effective reduction in the dimensionality of the electronic dispersion is also the proposed origin for the recent observation of NLMR in the interplanar resistivity of 2D correlated metals [40]. Remarkably, the appearance of the NLMR is not tied to the band structure of a particular material, but rather related to the type of scattering mechanism present in the system, and as in the classical model [37], ionized impurity scattering is proposed to give rise to a positive magnetoconductivity $\sigma \propto B^2$ [27]. Depending on the dominant contribution of the underlying scattering mechanisms, the magnetoconductivity may be temperature dependent, as observed in indium antimonide [39]. For Bi_2Se_3, we estimate that the quantum limit is reached at a field strength $B_0 \simeq 43$ T for the sample with the lowest carrier concentration of 1.2×10^{18} cm^{-3} (sample A) and thus our experiments lie outside the regime where a transition from a negative to a positive MR is proposed to occur due to short-range neutral impurity scattering [27].

In conclusion, we have investigated the MR response of thin Bi_2Se_3 epilayers. The low-temperature angle-dependent SdH data suggest a coexistence of bulk and surface charge carriers. At room temperature, we find a strong positive MR with a field dependence that can be explained by a field-dependent carrier mobility. The magnetoresistance itself is strongly anisotropic and depends on the orientation of the current I with respect to the parallel component of the magnetic field B. We have demonstrated that the observation of a NLMR akin to the axial anomaly is not specific to Dirac or Weyl semimetals, but may in fact occur in generic three-dimensional materials.

Part of this work has been supported by EuroMagNET II under EU Contract No. 228043 and by the Stichting Fundamenteel Onderzoek der Materie (FOM) with financial support from the Nederlandse Organisatie voor Wetenschappelijk Onderzoek (NWO). S.W. thanks NWO for his Veni grant (680-47-424) and acknowledges revealing discussions with B. A. Piot and M. Orlita.

[1] G. S. Nolas, J. Sharp, and H. J. Goldsmid, *Thermoelectrics* (Springer, New York, 1962).

[2] H. Zhang, C.-X. Liu, X.-L. Qi, X. Dai, Z. Fang, and S.-C. Zhang, Nat. Phys. **5**, 438 (2009).

[3] M. Z. Hasan and C. L. Kane, Rev. Mod. Phys. **82**, 3045 (2010).

[4] Y. Xia, D. Qian, D. Hsieh, L. Wray, A. Pal, H. Lin, A. Bansil, D. Grauer, Y. S. Hor, R. J. Cava, and M. Z. Hasan, Nat. Phys. **5**, 398 (2009).

[5] J. G. Analytis, R. D. McDonald, S. C. Riggs, J.-H. Chu, G. S. Boebinger, and I. R. Fisher, Nat. Phys. **6**, 960 (2010).

[6] D.-X. Qu, Y. S. Hor, J. Xiong, R. J. Cava, and N. P. Ong, Science **329**, 821 (2010).

[7] N. P. Butch, K. Kirshenbaum, P. Syers, A. B. Sushkov, G. S. Jenkins, H. D. Drew, and J. Paglione, Phys. Rev. B **81**, 241301(R) (2010).

[8] J. G. Analytis, J.-H. Chu, Y. Chen, F. Corredor, R. D. McDonald, Z. X. Shen, and I. R. Fisher, Phys. Rev. B **81**, 205407 (2010).

[9] M. Petrushevsky, E. Lahoud, A. Ron, E. Maniv, I. Diamant, I. Neder, S. Wiedmann, V. K. Guduru, F. Chiappini, U. Zeitler, J. C. Maan, K. Chashka, A. Kanigel, and Y. Dagan, Phys. Rev. B **86**, 045131 (2012).

[10] J. G. Checkelsky, Y. S. Hor, R. J. Cava, and N. P. Ong, Phys. Rev. Lett. **106**, 196801 (2011).

[11] D. Kim, S. Cho, N. P. Butch, P. Syers, K. Kirshenbaum, S. Adam, J. Paglione, and M. S. Fuhrer, Nat. Phys. **8**, 459 (2012).

[12] H. Köhler and H. Fischer, Phys. Status Solidi B **69**, 349 (1975).

[13] B. Fauqué, N. P. Butch, P. Syers, J. Paglione, S. Wiedmann, A. Collaudin, B. Grena, U. Zeitler, and K. Behnia, Phys. Rev. B **87**, 035133 (2013).

[14] M. Orlita, B. A. Piot, G. Martinez, N. K. S. Kumar, C. Faugeras, M. Potemski, C. Michel, E. M. Hankiewicz, T. Brauner, Č. Drašar, S. Schreyeck, S. Grauer, K. Brunner, C. Gould, C. Brüne, and L. W. Molenkamp, Phys. Rev. Lett. **114**, 186401 (2015).

[15] H. Tang, D. Liang, R. L. J. Qiu, and X. P. A. Gao, ACS Nano **5**, 7510 (2011).

[16] C. M. Wang and X. L. Lei, Phys. Rev. B **86**, 035442 (2012).

[17] X. Wang, Y. Du, S. Dou, and C. Zhang, Phys. Rev. Lett. **108**, 266806 (2012).

[18] H. He, B. Li, H. Liu, X. Guo, Z. Wang, M. Xie, and J. Wang, Appl. Phys. Lett. **100**, 032105 (2012).

[19] B. F. Gao, P. Gehring, M. Burghard, and K. Kern, Appl. Phys. Lett. **100**, 212402 (2012).

[20] M. Veldhorst, M. Snelder, M. Hoek, C. G. Molenaar, D. P. Leusink, A. A. Golubov, H. Hilgenkamp, and A. Brinkman, Phys. Status Solidi RRL **7**, 26 (2013).

[21] T. O. Wehling, A. M. Black-Schaffer, and A. V. Balatsky, Adv. Phys. **63**, 1 (2014).

[22] F. Arnold, C. Shekhar, S.-C. Wu, Y. Sun, R. Donizeth dos Reis, N. Kumar, M. Naumann, M. O. Ajeesh, M. Schmidt, A. G. Grushin, J. H. Bardarson, M. Baenitz, D. Sokolov, H. Borrmann, M. Nicklas, C. Felser, E. Hassinger, and B. Yan, Nat. Commun. **7**, 11615 (2016).

[23] M. Novak, S. Sasaki, K. Segawa, and Y. Ando, Phys. Rev. B **91**, 041203(R) (2015).

[24] J. Xiong, S. Kushwaha, J. Krizan, T. Liang, R. J. Cava, and N. P. Ong, Europhys. Lett. **114**, 27002 (2016).

[25] J. Xiong, S. K. Kushwaha, T. Liang, J. W. Krizan, W. Wang, R. J. Cava, and N. P. Ong, arXiv:1503.08179.

[26] J. Du, H. Wang, Q. Chen, Q. Mao, R. Khan, B. Xu, Y. Zhou, Y. Zhang, J. Yang, B. Chen, C. Feng, and M. Fang, Sci. China-Phys. Mech. Astron. **59**, 657406 (2016).

[27] P. Goswami, J. H. Pixley, and S. Das Sarma, Phys. Rev. B **92**, 075205 (2015).

[28] S. Schreyeck, N. V. Tarakina, G. Karczewski, C. Schumacher, T. Borzenko, C. Brüne, H. Buhmann, C. Gould, K. Brunner, and L. W. Molenkamp, Appl. Phys. Lett. **102**, 041914 (2013).

[29] See Supplemental Material at http://link.aps.org/supplemental/10.1103/PhysRevB.94.081302, which includes additional experimental data and a discussion concerning the two-carrier analysis.

[30] V. A. Kulbachinskii, N. Miura, H. Nakagawa, H. Arimoto, T. Ikaida, P. Lostak, and C. Drasar, Phys. Rev. B **59**, 15733 (1999).

[31] H. Köhler, Phys. Status Solidi B **58**, 91 (1973).

[32] S. Mukhopadhyay, S. Krämer, H. Mayaffre, H. F. Legg, M. Orlita, C. Berthier, M. Horvatić, G. Martinez, M. Potemski, B. A. Piot, A. Materna, G. Strzelecka, and A. Hruban, Phys. Rev. B **91**, 081105(R) (2015).

[33] L.-X. Wang, Y. Yan, L. Zhang, Z.-M. Liao, H.-C. Wu, and D.-P. Yu, Nanoscale **7**, 16687 (2015).

[34] X. Xu, A. F. Bangura, J. G. Analytis, J. D. Fletcher, M. M. J. French, N. Shannon, J. He, S. Zhang, D. Mandrus, R. Jin, and N. E. Hussey, Phys. Rev. Lett. **102**, 206602 (2009).

[35] D. Graf, J. S. Brooks, E. S. Choi, S. Uji, J. C. Dias, M. Almeida, and M. Matos, Phys. Rev. B **69**, 125113 (2004).

[36] J. Hu, M. M. Parish, and T. F. Rosenbaum, Phys. Rev. B **75**, 214203 (2007).

[37] In addition to the lateral sample sizes [length $L \times$ width W, $(30 \times 10)\ \mu\text{m}^2$] presented here, we have also measured samples with larger dimensions $(600 \times 200)\ \mu\text{m}^2$.

[38] P. N. Argyres and E. N. Adams, Phys. Rev. **104**, 900 (1956).

[39] R. Mansfield and T. Ellis, J. Phys. C: Solid State Phys. **9**, 3781 (1976).

[40] N. Kikugawa, P. Goswami, A. Kiswandhi, E. S. Choi, D. Graf, R. E. Baumbach, J. S. Brooks, K. Sugii, Y. Iida, M. Nishio, S. Uji, T. Terashima, P. M. C. Rourke, N. E. Hussey, H. Takatsu, S. Yonezawa, Y. Maeno, and L. Balicas, Nat. Commun. **7**, 10903 (2016).